JOURNAL OF MATERIALS SCIENCE **37** (2002) 3241 – 3249

Structural study of lithium titanium mixed oxides prepared by sol-gel process

M. PICQUART
Departamento de Física, Universidad Autónoma Metropolitana Iztapalapa, Apdo. Postal 55-534, México DF 09340, México

L. ESCOBAR-ALARCÓN
Departamento de Física, Instituto Nacional de Investigaciones Nucleares, Apdo. Postal 18-1027, México DF 11801, México

E. TORRES
Insituto de Materiales y Reactivos para la Electrónica (IMRE), Facultad de Química, Universidad de la Habana, San Lazaro y Vedado, La Habana 10400 Cuba

T. LOPEZ
Departamento de Química, Universidad Autónoma Metropolitana Iztapalapa, Apdo. Postal 55-534, México DF 09340, México

E. HARO-PONIATOWSKI*
Departamento de Física, Universidad Autónoma Metropolitana Iztapalapa, Apdo. Postal 55-534, México DF 09340, México
E-mail: haro@xanum.uam.mx

A structural study, using TGA-DSC analysis, X-ray diffraction, Raman scattering and FT Infrared absorption, is performed on mixed titanium lithium oxide with 20% of lithium prepared by sol-gel process. The structure is investigated as a function of the annealing temperature. At low temperatures the sample is in the anatase phase and transforms to the rutile phase near 500°C. The crystallite size of rutile TiO_2 increases from 40 to 100 nm as the temperature increases. However the size increase presents some discontinuity at temperature around 600°C. At thermal treatment temperatures from 500°C to 850°C the presence of $LiTi_2O_4$ in the sample is clearly observed. Finally at 1000°C the sample is composed by a mixture of rutile TiO_2 and $Li_2Ti_3O_7$.

1. Introduction

In the last years, the sol-gel techniques have received a lot of attention. Since the final characteristics of sol-gel samples depend on the precursors used in the initial solutions, materials with very specials requirements can be made. Titanium dioxide has been widely studied due to its various applications in: ceramics [1], coatings [2], thin films [3, 4], biomaterials [5], catalysts [6] or photocatalysts [7, 8] and chemical sensors [9, 10]. Titanium dioxide gels are obtained by hydrolysis and polymerization of an alkoxide in acid medium. During the preparation of the colloid, in the first step it is possible to add ions of alcalinous metals in a simple manner. These ions cogelify with the titanium alkoxide and take place in the colloid network [11]. Upon addition of these doping agents to titanium oxide, the physico-chemical properties are improved. In the same way it is possible to change the crystallinity depending on the doping ion size.

Titanium dioxide presents an amorphous phase and three crystalline phases: anatase, rutile and brookite, which are obtained by changing the reaction conditions and the doping agent [12]. Rutile is the most abundant phase in nature and corresponds to titanium octahedrically coordinated. Nevertheless when synthesized in laboratory the first phase observed is anatase [13].

Stoichiometric titanium dioxide (TiO_2) is a dielectric material, but it can be a semiconductor if the relation Ti/O = 1/2 is modified. The reaction mechanisms which give semiconductor properties to titanium oxide, where the important role of O–H groups is never forgotten, either as free radicals, adsorbed on the titanium oxide or simply by the excess of hydrogen which is generated inside the solid, which reacts easily with any specie in contact, is actually a subject of controversy. One of the simplest ways to obtain solids is by the sol-gel method, which gives a great number of O–H groups in the structure that create punctual defects [14]. Another way is by introducing an ion, which originates a variation of the band gap (E_g). The addition of alcalinous salts of metals to the samples during the gelation process, produces titanium oxide with a small part of

*Author to whom all correspondence should be addressed.

the metal M^+ in the network and the major part on the surface [14, 15]. It is then a potential catalyst and photocatalyst.

TiO_2/Li materials are good photocatalysts as they possess an adequate gap (2.7–3.1 eV) in order to decompose phenol with solar light [16]. Thermal treatment is provided in order to study the effect of deshydroxylation and expulsion of CO_3^{2-} ions. This is very important because it can generate defects in the solid giving semiconductor properties and a better photocatalyst behavior. Normally, at 600°C the solid has a great quantity of oxygen vacancies and is nearly completely deshydroxylated. When carbonyl ions are extracted near 900°C the porosity changes because the carbonate anion is big and its desorption causes a complete modification of texture.

In the present work, the lithium titanium oxide (20% in weight of Li) was obtained by sol-gel process involving metal-organic compounds (alkoxides) as precursors, which give a colloidal suspension and subsequently a gel [17–21]. The resulting gels obtained by this method present unusual properties. They possess stable structures at low temperatures, and thermal, structural and textural properties unobserved in traditional solids. The particle size lays in the nanoparticle domain [22–24]. Thermogravimetric analysis (TGA) and differential scanning calorimetry (DSC) of the TiO_2/Li gel followed by a structural analysis of TiO_2/Li gel at different annealing temperatures, from room temperature (RT) to 1000°C, by X-ray diffraction (XRD), Raman scattering and FT-IR absorption were used to characterize the obtained samples.

2. Experimental procedure

2.1. Sample preparation

Various methods of preparation of composite oxides exist, the mains are the following: (i) salts melting, (ii) coprecipitation, where one or more soluble salts are neutralized by the addition of a base inducing the coprecipitation of metallic oxide gels [25], (iii) impregnation, where the major component is mixed with a salt solution of the other metal, and the resulting suspension is slowly dried to obtain an homogeneous mixture [26–28], (iv) ionic exchange, where the less concentrated ion is in contact with an hydroxilated surface which carry out the proton exchange depending of the O─H bond nature [29].

In this paper the preparation of the sample is by sol-gel process. For the preparation of xerogels, two steps must be considered. The first, called pregelation, in which the alkoxides are hydrolyzed and condensed to form the gel. In this step the alkoxide oligomers form hydroxi (M─OH), alcoxi (R─OH) or ether (R─O─R) intermediate groups. The second step is the post gelation which initiates after the gelation point and includes all the phenomena that occur during the drying and calcination process: (i) water desorption, (ii) solvent evaporation, (iii) desorption of organic residues, (iv) deshydroxylation, and (v) structural and textural changes.

When the gelation occurs at alcalinous pH using NH_4OH as catalyst of hydrolysis, initial particles have an approximate diameter of 10 Å and their size increase with time [30]. This procedure gives mesoporous solids, these are amorphous initially and upon heating crystallize to anatase and rutile phases in the specific case of titanium oxide [31]. At pH 9 the reaction velocity of hydrolysis is lower than that of polymerization and linear gels are obtained [32].

The slow addition of titanium *n*-butoxide (alkoxide which is the titanium oxide precursor) to an homogeneous solution of lithium carbonate which is in reflux and constant stirring, gives rise to an uniform nucleation of the involved species. Initially, the lithium carbonate is dissociated in Li^+ and CO_3^{2-} which results into electrostatic repulsions with the carbonate ion, but a strong attraction with the lithium cation:

$$\mathrm{M(OR)_4 + H_2O \xrightarrow{NH_4OH} (RO)_3\,M{-}O^- + ROH}$$
$$\mathrm{\xrightarrow{Li^+} (RO)_3\,M{-}O{-}Li + ROH} \quad (1)$$

Nevertheless these repulsions and attractions of the components give an homogeneous distribution of lithium in the titanium oxide and a 100% superficial dispersion of the alcalinous metal (Li_2O) which combines with titanium oxide to form $LiTi_2O_4$ as it was shown by the Rietveld method [16].

The crystal structure and crystallite size are direct functions of the thermal treatment temperature. Both properties are of great importance in the behavior of the material when it is used as catalyst or as active compound for special ceramics.

In the present case the samples were prepared using the following procedure: in a flask, 150 ml of ethanol (Baker, 99.9%) were refluxed at 70°C. Under constant stirring, NH_4OH (Baker, 35% NH_3 in water) were added to adjust the pH at 9. A solution of 72.2 ml of titanium *n*-butoxide (Aldrich, 99.9%) in 100 ml of ethanol and 35 ml of an aqueous solution of Li_2CO_3 (Baker, 99.99%) was added dropwise during 2 1/2 hours until a final concentration of 20% of Li atoms in weight was obtained. The mixture was left under both stirring and refluxing until the gels were formed. The as-prepared material was a white powder. The thermal treatments were done by heating the samples during two hours at the desired temperature in a thermally regulated Lindberg oven.

2.2. Thermal analysis

Thermogravimetric analysis (TGA) and differential scanning calorimetry (DSC) of the TiO_2/Li gel were performed simultaneously on a Netzch STA-409 EP by linearly heating (10°C/min) in a static air atmosphere.

2.3. Powder X-ray diffraction (XRD)

The X-ray diffraction patterns were obtained using a Siemens D-5000 diffractometer with a Cu K_α radiation source ($\lambda_k = 1.5406$ Å). The average crystallite size was calculated by the Scherrer equation.

2.4. Raman scattering spectroscopy

The Raman scattering experiments were performed at room temperature on a computerized Spex 1403 double

monochromator, using a Lexel Ar^+ laser. We used the 514.5 nm laser line with a power of 100 mW at the laser head and the spectral resolution was about 2 cm^{-1}. The scattered light, detected in a backscattering geometry, was collected on the photocathode of a cooled photomultiplier, followed by a standard photon counting system. The same thermally treated samples as those used for X-ray diffraction were analyzed by Raman scattering.

2.5. Infrared absorption measurements

Samples for FT-IR measurements were made by mixing TiO_2/Li powder in KBr pellets. FT-IR spectra were recorded on a Perkin Elmer 1600 FT-IR spectrometer equipped with a globar source and a TGS (triglycine sulfate) detector. In order to eliminate the spectral contributions of the atmospheric water vapor and carbon dioxide, the instrument was purged with dry air. For each spectrum, 40 interferograms at 4 cm^{-1} resolution were collected, co-added, apodized with a Happ-Genzel function and Fourier transformed. The same thermally treated samples as those used for X-ray diffraction and Raman scattering were used for FT-IR.

3. Results and discussion

3.1. Thermal analysis

In Fig. 1 are presented the TGA and the DSC curves of the TiO_2/Li gel. Two mass losses are observed: (i) the most important appears between 120 and 150°C followed by a slow decrease up to 500°C with a total mass loss of 22%; (ii) the second one between 800 and 1000°C with a 3% mass loss. At the same time the DSC curve presents at least 5 important processes: three endothermic at 155, 475 and 602°C and two exothermic at 551 and 971°C.

The first endothermic peak, correlated to the main mass loss, corresponds to the physisorbed water and solvent loss in the material. The second endothermic peak at 475°C is due to a partial deshydroxylation of the titania and is correlated to the slow decrease of mass. This process is associated with a superficial free energy liberation by the breaking of Ti—OH bonds and formation of new Ti—O—Ti bonds which increase the particle size. The last endothermic peak (602°C) shows that the deshydroxylation process is still going on. The first exothermic peak at 551°C is due to the anatase → rutile phase transition of the titanium oxide. The last exothermic peak is due to carbonates decomposition releasing carbonyl groups and is correlated to the second mass loss. Normally this process occurs at lower temperatures (618°C), nevertheless by this sol-gel method the carbonates are retained in the material to higher temperatures [33]. This carbonates decomposition suggests a solid state reaction between the lithium which is product of the decomposition and the titanium oxide, which results in the formation of a new oxide.

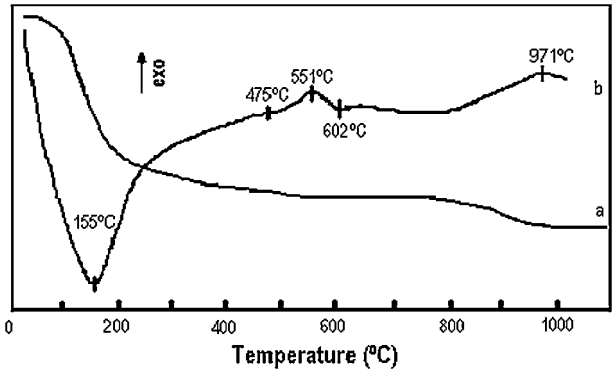

Figure 1 Thermogravimetric (a) and DSC (b) curves.

As we have seen on the DSC and thermogravimetric analysis, the anatase to rutile phase transition is completed approximately at 550°C in good agreement with a previous work [31] on TiO_2 nanoparticles. It seems that lithium has not a detectable effect on the anatase to rutile transition, as opposed to other dopants [34]. Nevertheless a new oxide due to the presence of lithium appears at high temperature.

3.2. X-ray powder diffraction

Fig. 2 shows the XRD patterns of untreated powder (RT) together with the thermally treated powders at different temperatures (300, 370, 400, 500, 650, 700, 850 and 1000°C). The XRD pattern of the untreated powder (RT) consists of broad bands peaking at $2\theta = 25°$, 31°, 38°, 48°, 55°, 64°, 70° and 76°. This spectrum reveals that this sample consists of a mixture of anatase and brookite, with anatase as the predominant phase. After a thermal treatment at 300°C the presence of a small broad peak centered at $2\theta = 27.5°$ is observed. This peak indicates that the rutile phase begins to appear at this temperature. Upon annealing at 370°C part of the powder crystallizes in the rutile phase. This is indicated by the presence of some peaks at $2\theta = 27.5°$, 36.1°, 41.2°, 54.3° and 56.6° characteristic of this TiO_2 phase as observed on the corresponding spectrum. At 370°C the sample is composed approximately of 56% rutile and 44% anatase. If a thermal treatment at 400°C is applied, the obtained sample consists predominantly of rutile (94%) with a small quantity of anatase. This rutile-anatase relation is indicative of the phase transition anatase → rutile. The difference with DTA results probably comes from the rate heating process which is faster in the case of DTA than in the case of X-ray analysis.

When the sample is thermally treated at 500°C, it completely crystallizes into the rutile phase as observed in the corresponding diffractogram presented in Fig. 2. This diffractogram has peaks at $2\theta = 27.5°$, 36.1°, 41.2°, 44°, 54.3°, 56.6°, 62.7°, 64°, 69° and 69.8° that correspond unambiguously to the rutile TiO_2 phase.

At thermal treatment temperatures from 500°C to 850°C the diffraction patterns corresponding to the rutile TiO_2 are obtained. This is indicated by the presence of the rutile peaks shown in Fig. 2. However an additional peak at $2\theta = 18.2°$ attributed to the presence of $LiTi_2O_4$ in the sample is clearly observed. This new peak increases in intensity at temperatures from

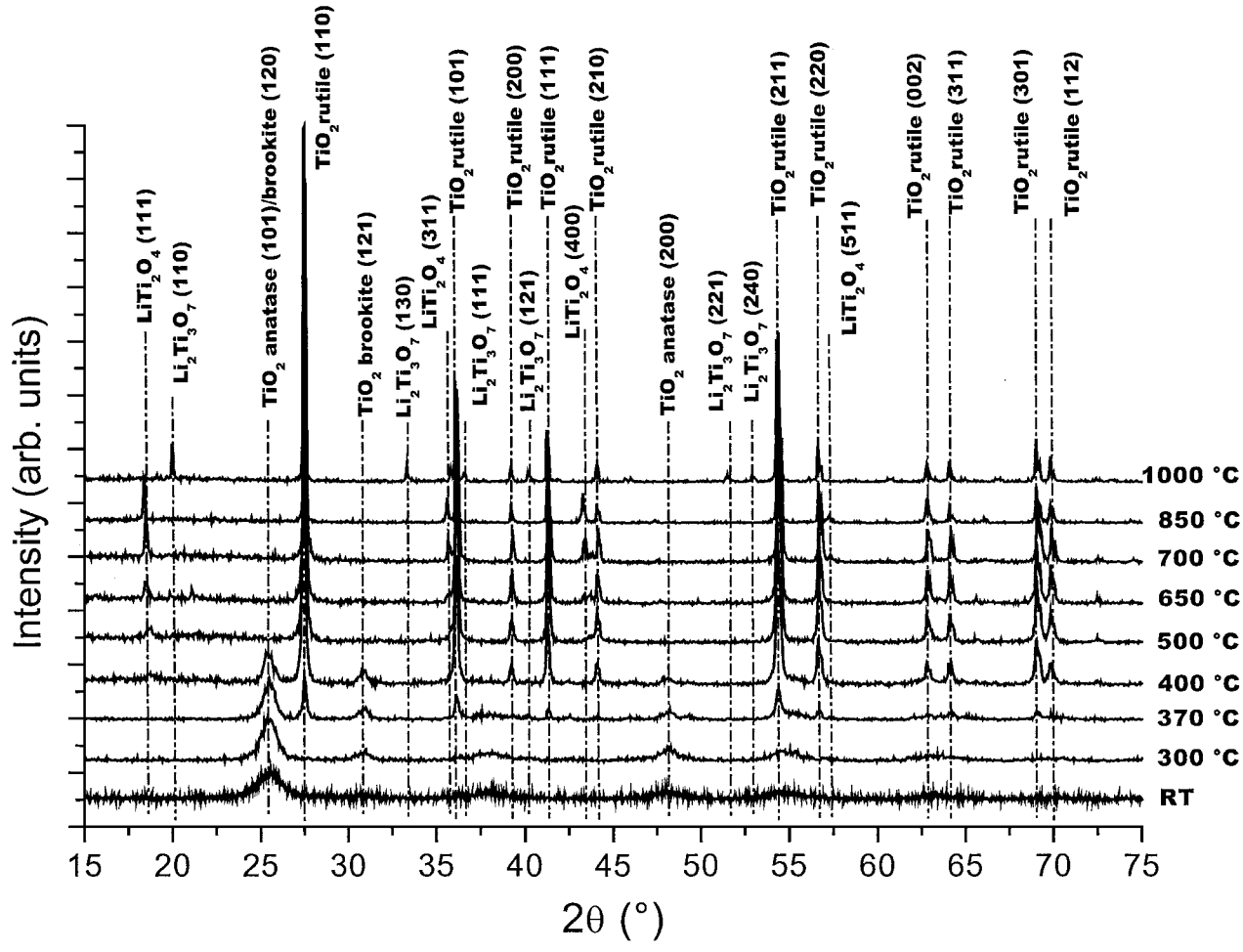

Figure 2 XRD patterns at different annealing temperatures.

500°C to 850°C indicating that this specie increases in quantity. Even more at temperatures in the range from 500°C to 850°C the sample consists of a mixture of rutile TiO_2 and $LiTi_2O_4$ with rutile as the major phase.

Finally at 1000°C the presence of additional new peaks are clearly observed. These peaks are centered at $2\theta = 20°$, 33.3°, 35.8°, 36.5°, 40.2°, 51.5° and 52.9c, corresponding to $Li_2Ti_3O_7$. At 1000°C the sample is composed by a mixture of rutile TiO_2 and $Li_2Ti_3O_7$. The existence of the new oxide is correlated by the DSC measurements as seen above. It's worth noting that at 1000°C the $LiTi_2O_4$ phase disappears completely. It should be noted that pure titania is a good photocatalyst for the 2,4 dinitro-aniline. However addition of lithium resulting in the formation of $LiTi_2O_4$ improves significantly this property [35].

From the sequences showed in Fig. 2 it is clearly observed that as the thermal treatment temperature increases, the peaks associated with the rutile phase become sharper and more intense indicating that the crystallinity of the rutile phase has improved markedly. For this phase the crystallite size was estimated using the Scherrer equation:

$$D = \frac{0.9\lambda}{\beta \cos\theta} \tag{2}$$

where λ is the X-ray wavelength, θ is the Bragg angle and β is the pure full width of the diffraction line at half of the maximum intensity using the peak at 27.5°.

The average crystallite sizes as a function of the thermal treatment temperature are shown in Fig. 3. Using a simple Arrhenius equation of the type [36]:

$$D = D_0 \, \mathrm{e}^{-\frac{E_a}{kT}} \tag{3}$$

It is not possible to find an unique activation energy E_a for the full range of annealing temperatures. In the present case we have fitted our data with two different straight lines. The first having an activation energy of 0.05 eV and a D_0 of 361 nm covers the low temperature range. For the high temperature range the value of E_a and D_0 are 0.13 eV and 126 nm, respectively. The intersection of the two lines occurs around 620°C. The change of the growth rate of the nanoparticles could be related to the appearance of the $LiTi_2O_4$ compound however further investigations are needed to clarify this behavior.

3.3. Raman scattering spectroscopy

In Fig. 4 the Raman spectra in the 50–950 cm^{-1} region of the titanium lithium oxide samples at different annealing temperatures from room temperature to 850°C are presented. Between room temperature and 370°C,

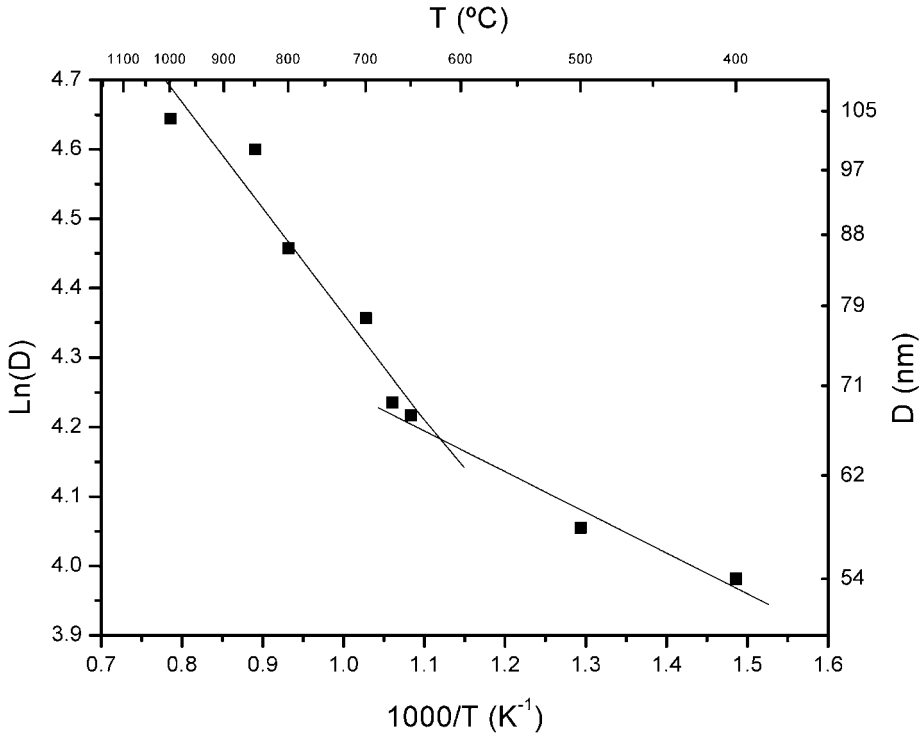

Figure 3 Crystallite size of the TiO_2 as function of the annealing temperature.

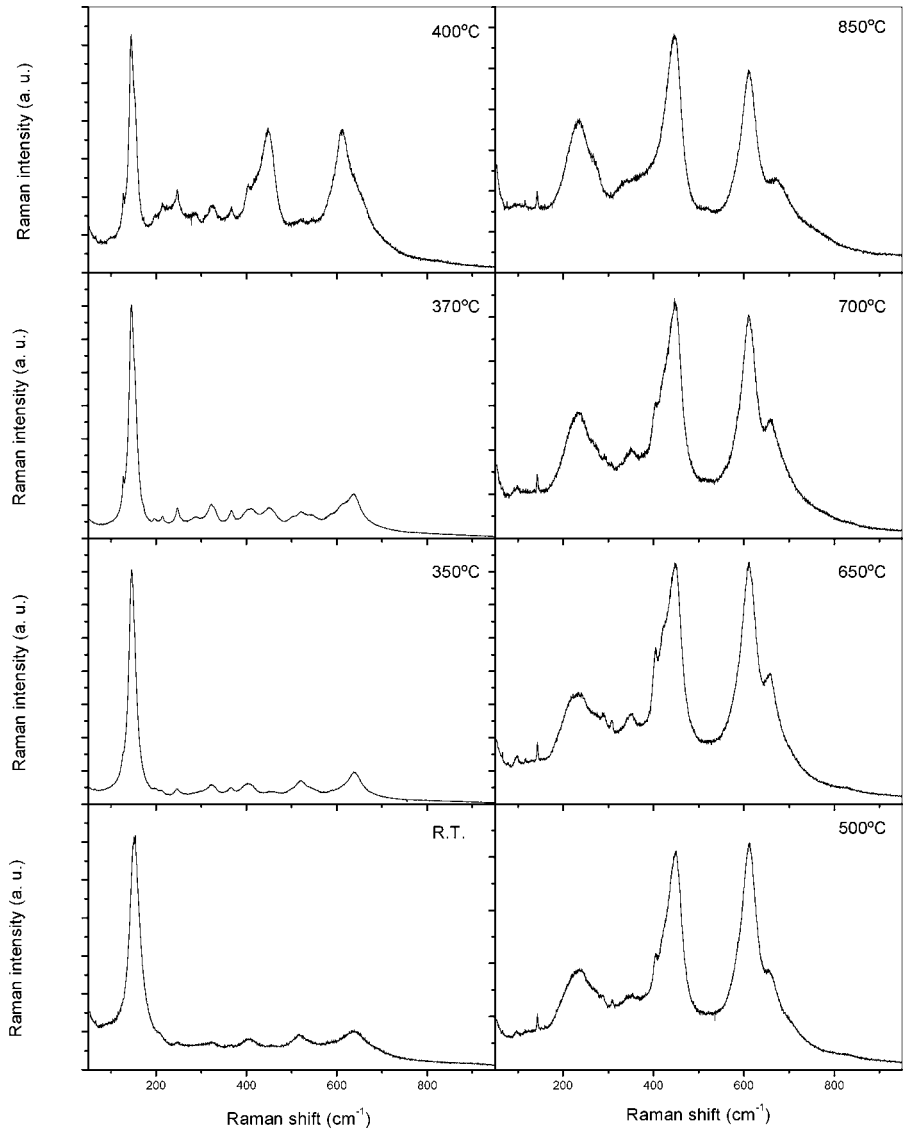

Figure 4 Raman spectra of the TiO_2/Li at different annealing temperatures in the 50–950 cm^{-1} region.

TABLE I Raman frequencies of the mixed TiO_2/Li oxide at different annealing temperatures in the 50–950 cm^{-1} region

RT	350°C	370°C	400°C	500°C	650°C	700°C	850°C	Assignment
				96	98	96	101 vw	
	127	127	127					A_{1g} Brookite
151	146	146	145					E_g Anatase
				142 w	142 w	142 w	142 w	B_{1g} Rutile
			153 sh					A_{1g} Brookite
	198 vw	197	198 vw					Eg An. A_{1g} Br.
	213 vw	214	213					B_{1g} Brookite
				236	234	233	231	Rut. Dis or 2nd ord.
248	248	248	248					A_{1g} Brookite
		288	286	278 sh	289	278 sh	269 sh	$LiTi_2O_4$
325	322	322	325	320 vw	320			B_{1g} Brookite
363vw	366	368	366					B_{2g} Brookite
				353	351	351		$LiTi_2O_4$
406	404	407	404 sh	405 sh	404	401 sh		B_{1g} An. A_{1g} Br.
			420 sh	422 sh	422 sh	422 sh		$LiTi_2O_4$
			448	449	448	448	447	Eg Rutile
454 vw	456	451						B_{3g} Brookite
		503 sh						A_{1g} An. B_{1g} Br.
518	521	521	521 vw					A_{1g} An. B_{1g} Br.
	546 sh	542 sh	547 vw					
		589 sh						
		612 sh	612	612	612	612	612	A_{1g} Rutile
638	638	638						E_g An. A_{1g} Br.
			650 sh	657	656	659	671	$LiTi_2O_4$

sh, shoulder; vw, very weak; An, anatase; Br, brookite.

the samples are characterized by a strong vibration at 146 cm^{-1} and small bands at 127, 198, 213, 248, 322, 366, 404, 456, 521, 546 and 638 cm^{-1}. All the observed vibration modes with their possible attribution are reported in Table I.

It is well known [37–40] that a strong band near 145 cm^{-1} and small bands near 198, 395, 514 and 638 cm^{-1} are signature of anatase phase. The weak bands that appear at 127, 248, 322, 366 and 456 cm^{-1} on the sides of the anatase bands indicates that there is also a small quantity of brookite phase [39, 40]. This result is in accordance with the X rays results described above. It can be observed that from 500 to 1000°C the sample is in part in the rutile phase as indicated by the strong bands at 233, 446, 610, and a weak band at 827 cm^{-1}. Many of the bands attributed to vibrations of the brookite phase have disappeared at 500°C, nevertheless the small band at 320 cm^{-1} still appears at 650°C and another one at 401 cm^{-1} is still present at 700°C. Above 850°C the Raman spectra corresponds closely to TiO_2 in the rutile phase however some small bands that appear peaking at 101, 270, 351, 422 and 660 cm^{-1} between 370 and 850°C are unknown in the Raman spectra of anatase, brookite and rutile. In order to assign these bands, a powder of $LiTi_2O_4$ was prepared. The Raman spectrum (spectrum not shown) shows bands at: 144, 235, 271, 355, 415, 447, 612, 676 and 760 cm^{-1}. The bands observed at 270, 351, 422 and 660 cm^{-1} at temperatures above 370°C could be attributed to the $LiTi_2O_4$ phase that was observed in small quantity in the XRD patterns.

When the same compound is thermally treated at 1000°C, we can observe a change in the part of the spectrum below 200 cm^{-1} (spectrum not shown). Bands at 126 and 161 cm^{-1} appear that were not observed in the spectrum at 850°C (Fig. 4) and could probably be due to the new oxide ($Li_2Ti_3O_7$) observed at 1000°C by XRD and suggested by DSC results.

From Raman scattering we observe the intense band of anatase between 151 and 145 cm^{-1}. Music *et al.* [40] have shown that a Raman shift higher than 142 cm^{-1}, could be due to the vibrational mode of nano-sized particles.

3.4. Infrared absorption

In Fig. 5 are presented the FT-IR absorption spectra in the 250–3850 cm^{-1} region of the TiO_2/Li samples at different annealing temperatures. All the infrared absorptions in this frequency range are reported in Table II. At room temperature, the FT-IR spectrum is characterized by a very strong absorption band centered near 600 cm^{-1} with maxima at 480, 598 and 735 cm^{-1}. These absorptions are assigned to $\nu_{Ti—O}$ (550–653 cm^{-1}) and $\delta_{Ti—O—Ti}$ (436–495 cm^{-1}), respectively [41, 42]. At lower frequency a strong and sharp absorption is observed (343 cm^{-1}).

At higher frequency two strong and sharp absorptions are observed at 1399 and 1632 cm^{-1} which are probably due to the carbonate stretching vibrations and to the bending mode of adsorbed water, respectively. In some spectra very weak absorptions are observed near 2859 and 2926 cm^{-1} corresponding to C—H stretching vibrations due to residual titanium *n*-butoxide chain used in the preparation. Two very strong absorptions at higher frequencies are observed at 3216 and 3405 cm^{-1} at room temperature corresponding to $\nu_{O—H}$ stretching modes of water occluded in the titania network, to some alcohol residues and to hydroxy groups (Ti—OH) bound to the titanium atoms. This part of the spectrum is analogous to that of pure water [43] and indicates that is mainly due to residual crystallization water.

TABLE II Infrared absorption bands of the mixed TiO_2/Li oxide at different annealing temperatures in the 250–3850 cm^{-1} region

RT	300°C	350°C	400°C	500°C	650°C	700°C	850°C	Assignment
343	343	343	343	343	343	343	343	
			419	409	414	414	414	$\delta_{Ti—O—Ti}$
480	492	492						$\delta_{Ti—O—Ti}$
	553	548	548	537	542	542	531	$\nu_{Ti—O}$
598	598	603						
			648	670	650	653	636	$\nu_{Ti—O}$
735		715					731	
			870	870				δ_{CO}
				904			909	
	1120	1126					1159	
1399	1399	1399	1399	1399	1399	1399	1399	ω_{CH}
			1438	1438				γ_{CO}
			1499	1499	1510			γ_{CO}
1632	1627	1627	1632		1632	1630	1632	δ_{OH}
	1654	1655	1655	1650				
2859	2859	2859	2859	2853	2853	2865	2859	ν_{CH}
2926	2932	2432	2926	2920	2920	2937	2926	ν_{CH}
3020		3015	3015		3015	3015	3015	ν_{CH}
3216	3204	3149	3171	3199	3137	3143	3154	ν_{OH}
3405	3394	3399	3404	3432	3388	3443	3426	ν_{OH}

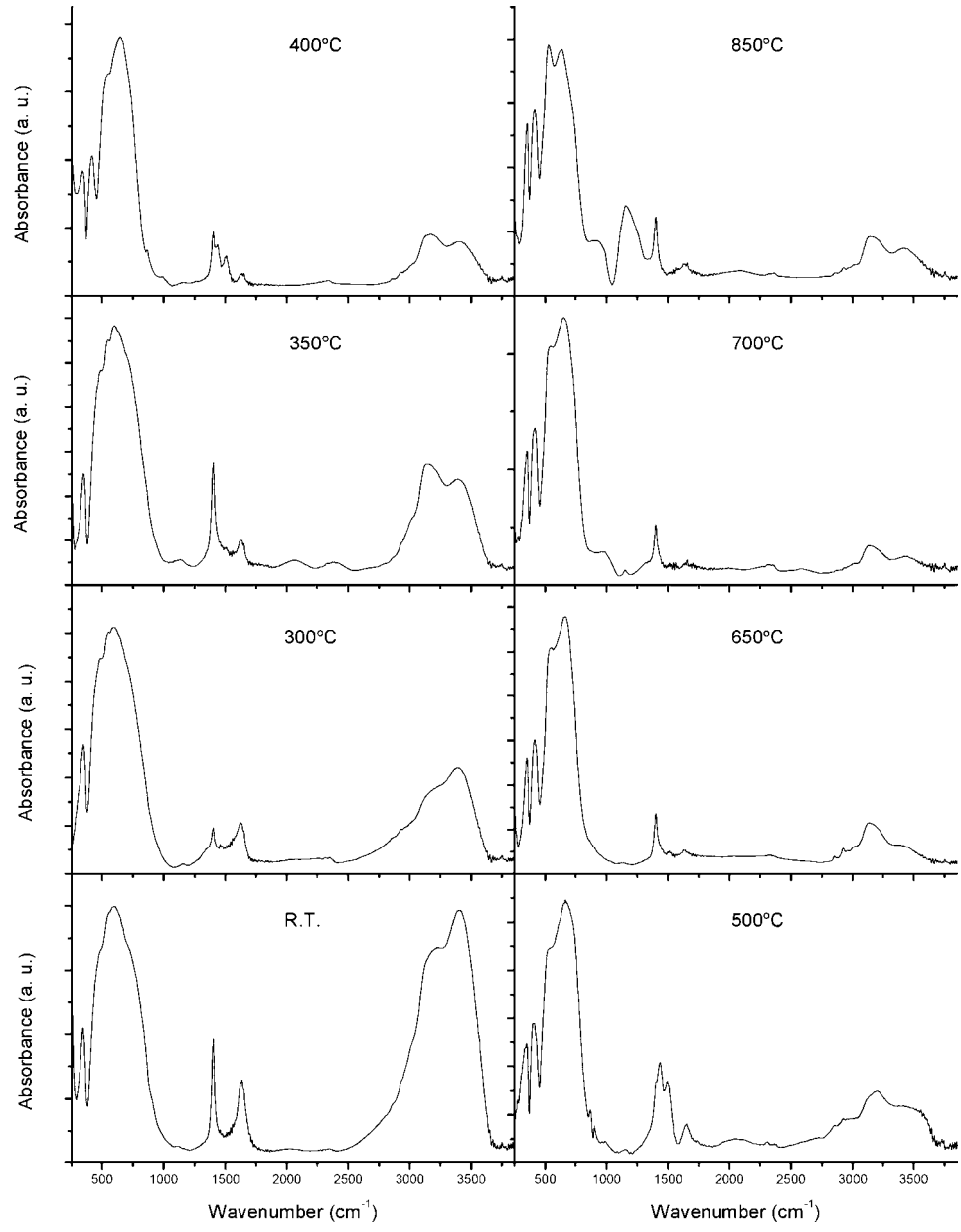

Figure 5 FT-IR absorption spectra of the TiO_2/Li samples at different annealing temperatures in the 250–3850 cm^{-1} region.

At 300°C, the spectrum does not change except that a loss of water can be observed. At 350°C, the absorption spectrum has changed in this region. The more intense band is the 3149 cm^{-1} one, showing that the residual OH are mainly due to Ti—OH bonds. Up to 850°C, the intensity of this band diminishes slowly indicating the slow desydroxylation observed by TGA and DSC measurements.

At the same time a first phase transition is observed on the 400°C spectrum, where absorptions near 419, 648 cm^{-1} are observed and those observed near 492 and 603 cm^{-1} have vanished. These absorptions are assigned to bending and stretching modes of Ti—O—Ti in the rutile and anatase phases, respectively.

Small absorption bands appear on the spectrum at 400 and 500°C near 870, 1438 and 1499 cm^{-1}. These bands are observed when the anatase → rutile phase transition occurs and disappear at higher temperatures. These are probably due to δ_{CO} and γ_{CO} vibrations of carbonates. As the carbonates decomposition occurs these bands vanish.

From FT-IR measurements Ocaña *et al*. [37] have shown that the IR spectrum can vary with the size of the particle. They have shown that the absorptions near 650 and 540 cm^{-1} correspond to two different morphologies, i.e., spheres and oblate spheroids, respectively. But they did not discard that the 540 cm^{-1} absorption could be due to spheres with a high state of aggregation.

At 850°C a small change is observed in the low frequency region where the band at 531 cm^{-1} has a higher intensity than the band at 636 cm^{-1}. We can also observe a strong absorption at 1159 cm^{-1}. The same characteristics are observed on the $LiTi_2O_4$ powder in agreement with Raman results. At 1000°C (spectrum not shown) the obtained spectrum is almost identical to the one obtained at 850°C, but the Ti—OH stretching bands are at 3131 and 3413 cm^{-1}.

4. Conclusion

TiO_2/Li gels were obtained by sol-gel process. DSC, XRD, Raman and FT-IR results are in agreement and have shown that the structure of the fresh material is in the anatase phase. The gels still contain some residuals of the sol-gel process as shown by FT-IR. XRD spectra show that the mean crystallite size increases from 40 to 105 nm as a function of the annealing temperature.

Acknowledgments

One of the authors (M.P.) thanks the Universidad Autónoma Metropolitana Iztapalapa and the Consejo Nacional de Ciencias y Tecnología (CONACyT) of México for financial support.

References

1. L. L. HENCH and D. R. ULRICH, in "Ultrastructure Processing of Ceramic Glasses and Composites" (Wiley, New York, 1984).
2. S. SAKKA, in "Treatise on Materials Science and Technology," Vol. 22 (Academic Press, New York, 1982) p. 129.
3. L. C. KLEIN, in "Sol-Gel Technology for Thin Films, Fibers, Preforms, Electronics and Speciality Shapes" (Noyes Publications, New Jersey, 1988).
4. L. ESCOBAR-ALARCÓN, E. HARO-PONIATOWSKI, M. A. CAMACHO-LÓPEZ, M. FERNÁNDEZ-GUASTI, J. JÍMENEZ-JARQUÍN and A. SÁNCHEZ-PINEDA, *Appl. Surf. Sci*. **137** (1999) 38.
5. B. E. YOLDAS, *J. Mater. Sci*. **63** (1980) 1765.
6. T. LÓPEZ and R. GÓMEZ, in "Sol-Gel Optics—Processing and Applications" (Kluwer Academic Publishers, Norwell, 1994) ch. 16.
7. E. SANCHEZ, T. LÓPEZ, R. GÓMEZ, X. BOKHIMI, A. MORALES and O. NOVARO, *J. Solid State Chem*. **122** (1996) 309.
8. L. ZANG, C.-Y. LIU and X. M. REN, *J. Chem. Soc. Faraday Trans*. **91** (1995) 917.
9. J. SYKORA, *Coord. Chem. Rev*. **159** (1997) 95.
10. A. SALMA-SCHWOK, D. AVNIR and M. OTTOLENGHI, *J. Phys. Chem*. **93** (1989) 7544.
11. R. D. GONZALEZ, T. LÓPEZ, R. GÓMEZ, *Catalysis Today* **35** (1997) 293.
12. M. GOTIC, M. IVANDA, A. SEKULIC, S. MUSIC, S. POPOVIC, A. TURKOVIC and K. FURIC, *Matt. Lett*. **28** (1996) 225.
13. International Tables for Crystallographie, Vol. IV (Kynoch Press, Birmingham, 1974).
14. L. MANZANI, G. ANTONIELI, D. BERSANI, P. P. LOTTICI, G. GNAPPI and A. MONTENERO, *J. Non. Cryst. Solids* **192** (1995) 519.
15. J. C. CONESA and J. SORIA, *J. Phys. Chem*. **86** (1982) 1392.
16. T. LÓPEZ, J. HERNANDEZ-VENTURA, R. GÓMEZ, F. TZOMPANTZI, E. SANCHEZ, X. BOKHIMI and A. GARCIA, *J. Mol. Cat*. A: *Chemical* **1** (2000) 2995.
17. G. M. PAJONK, *Appl. Catal*. **72** (1991) 217.
18. T. LÓPEZ, I. GARCIA-CRUZ and R. GÓMEZ, *J. Catal*. **127** (1991) 75.
19. L. C. KLEIN, *Ann. Rev. Mat. Sci*. **15** (1985) 227.
20. T. LÓPEZ, R. GÓMEZ, G. PECCI, P. REYES, X. BOKHMI and O. NOVARO, *Matt. Lett*. **40** (1999) 59.
21. T. LÓPEZ, O. CHIMAL, M. ASOMOZA, R. GÓMEZ, X. BOKHIMI, O. NOVARO and R. D. GONZALEZ, *J. Solid State Chem*. **144** (1999) 349.
22. G. PECCI, P. REYES, T. LÓPEZ and R. GÓMEZ, *Appl. Catal*. A **17** (1998) 7.
23. T. LÓPEZ, F. TZOMPANTZI, J. NAVARRETE, R. GÓMEZ, J. L. BOLDU, E. MUÑOZ and O. NOVARO, *J. Catal*. **181** (1999) 285.
24. T. LÓPEZ, R. GÓMEZ, J. NAVARRETE and E. LÓPEZ-SALINAS, *J. Sol-Gel Sci. Tech*. **13** (1998) 317.
25. W. ZOU and R. D. GONZALEZ, *Catal. Lett*. **12** (1992) 73.
26. M. VINIEGRA, R. GÓMEZ and R. D. GONZALEZ, *J. Catal*. **111** (1988) 429.
27. T. LÓPEZ, P. BOSCH, M. MORÁN and R. GÓMEZ, *J. Phys. Chem*. **97** (1993) 1671.
28. C. SANCHEZ and J. LIVAGE, *New J. Chem*. **14** (1990) 513.
29. K. TANABE, *Mater. Chem. Phys*. **13** (1985) 347.
30. C. J. BRINKER and G. W. SCHERER, *J. Amer. Ceram. Soc*. **69** (1986) 12.
31. E. HARO-PONIATOWSKI, R. RODRÍGUEZ-TALAVERA, M. DE LA CRUZ HEREDIA, O. CANO-CORONA and R. ARROYO-MURILLO, *J. Mater. Res*. **9** (1994) 2102.
32. A. J. BARD, *J. Phys. Chem*. **86** (1982) 172.
33. J. L. BOLDU, E. MUNOZ, X. BOKHIMI, O. NOVARO, T. LOPEZ and R. GOMEZ, *Langmuir* **15** (1999) 32.
34. S. VARGAS, R. ARROYO, E. HARO and R. RODRÍGUEZ, *J. Mater. Res*. **14** (1999) 3932.
35. T. LÓPEZ, J. HERNÁNDEZ-VENTURA, R. GÓMEZ, F. TZOMPANTZI, E. SÁNCHEZ, X. BOKHIMI and A. GARCÍA, *J. Mol. Catal. A: Chemical* **167** (2001) 110.
36. M. JOUANNE, J. F. MORHANGE, M. KANEHISA, E. HARO-PONIATOWSKI, G. A. FUENTES, E. TORRES and E. HERNÁNDEZ-TELLEZ, *Phys. Rev*. B **64** (2001) 155404.
37. M. OCAÑA, V. FORNÉS, J. V. GARCIA RAMOS and C. J. SERNA, *J. Solid State Chem*. **75** (1988) 364.
38. M. OCAÑA and C. J. SERNA, *Spectrochimica Acta* **47A** (1991) 765.

39. G. A. TOMPSETT, G. A. BOWMAKER, R. P. COONEY, J. B. METSON, K. A. RODGERS and J. M. SEAKINS, *J. Raman Spectr*. **26** (1995) 57.
40. S. MUSIC, M. GOTIC, M. IVANDA, S. POPOVIC, A. TURKOVIC, R. TROJKO, A. SEKULIC and K. FURIC, *Mat. Sc. Engin*. B **47** (1997) 33.
41. A. LARBOT, I. LAAZIZ, J. MARIGNAN and J. F. QUINSON, *J. Non-Crystall. Solids* **147/148** (1992) 157.
42. K. CHLOR, J. F. BOCQUET and C. POMMIER, *Mater. Chem. Phys*. **32** (1992) 249.
43. G. E. WALRAFEN, in "Water—A Comprehensive Treatise," Vol. 1 (Plenum, New York, 1972) ch. 1.

Received 11 June 2001
and accepted 17 April 2002